Eur. Phys. J. B (2018) 91: 152
https://doi.org/10.1140/epjb/e2018-90223-5

THE EUROPEAN PHYSICAL JOURNAL B

Regular Article

Pulse shape and molecular orientation determine the attosecond charge migration in Caffeine*

Thomas A. Niehaus[1,a], Mehdi Meziane[1], Franck Lepine[1], Alexandre Marciniak[1], Kaoru Yamazaki[2], and Hirohiko Kono[3]

[1] Univ. Lyon, Université Claude Bernard Lyon 1, CNRS, Institut Lumière Matière, 69622 Villeurbanne, France
[2] Tohoku University, Institute for Materials Research, 980-8577 Sendai, Japan
[3] Department of Chemistry, Graduate School of Science, Tohoku University, Sendai 980-8578, Japan

Received 3 April 2018
Published online 4 July 2018

Abstract. The recent reduction of laser pulse duration down to the attosecond regime offers unprecedented opportunities to investigate ultrafast changes in the electron density before nuclear motion sets in. Here, we investigate the hole dynamics in the Caffeine molecule that is induced by an ionizing XUV pulse of 6 fs duration using the approximate time-dependent density functional theory method TD-DFTB. In order to account for ionization in a localized atomic orbital basis we apply a complex absorbing potential to model the continuum. Propagation of the time-dependent Kohn–Sham equations allows us to extract the time-dependent hole density taking the pulse shape explicitly into account. Results show that the sudden ionization picture, which is often used to motivate an uncorrelated initial state, fails for realistic pulses. We further find a strong dependence of the hole dynamics on the polarization of the laser field. Notwithstanding, we observe fs charge migration between two distant functional groups in Caffeine even after averaging over the molecular orientation.

1 Introduction

Time-dependent density functional theory (TD-DFT) [1], as pioneered by Eberhard Groß, had an impact on the modeling of electronic excited states that is difficult to overestimate. Typical applications range from the routine determination of molecular absorption spectra (where TD-DFT has become an in-silico characterization tool even for experimental chemists), over the investigation of charge transfer in photovoltaic and energy conversion materials [2], up to the real-time observation of carrier dynamics in solids [3].

Meanwhile, progress in the development of ultrashort lasers sources brought the experimentally accessible time scales down to a regime that can be easily dealt with in TD-DFT simulations. The transition of ps to fs laser pulses marked the advent of femtochemistry [4], which enabled the tracking of nuclear motion. More recently, attosecond (as) XUV laser pulses obtained from high-harmonic generation can even elucidate the faster electron dynamics in pump-probe experiments on molecules of increasing complexity [5–9].

One of the genuine electronic phenomena that received a lot of attention in this context is termed *charge migration* [10], which is the few or sub-fs oscillation of positive charge along a molecular backbone. The effect is initiated by an ionizing laser pulse that prepares the system in a non-stationary state. If the cationic wave function can be written as a superposition of molecular orbitals of largely differing localization, the resulting hole dynamics might feature nearly instantaneous displacements over large distances. The experimental detection of charge migration is difficult since it requires an exceptional degree of temporal and spatial resolution. It is typically performed in an indirect fashion recording for example the shift in site specific absorption spectra [6] or molecular fragment distributions [9]. Theoretical simulations are called for in such a situation and, in fact, early calculations by Cederbaum and co-workers elucidated the principle origin of charge migration [10–12]. In many later studies it was assumed that the state right after ionization can be approximated by a single determinant for the neutral molecule from which a given molecular orbital is removed to imitate the *sudden ionization* by high energy pulses [12–14]. This is questionable especially in the DFT context, where the physical meaning of the auxiliary Kohn–Sham orbitals is rather unclear. More important is the fact that the choice which orbital to remove needs to be based on the actual pulse profile and the detailed ionization probabilities. Efforts towards the construction

* Contribution to the Topical Issue "Special Issue in honor of Hardy Gross", edited by C.A. Ullrich, F.M.S. Nogueira, A. Rubio, and M.A.L. Marques.

[a] e-mail: thomas.niehaus@univ-lyon1.fr

of more realistic initial states beyond the single-particle picture have been put forward only recently [15].

In this contribution, we follow this direction and present a method to quantify charge migration that is completely formulated in the time domain and takes the temporal pulse profile fully into account. The working equations are given for conventional TD-DFT in an atomic orbital basis. The implementation and later numerical simulations are however carried out using TD-DFTB, a more approximate variant of TD-DFT to speed up the calculations. One consequence of including the actual laser field is that the hole dynamics are influenced by the molecular orientation, a fact that has not been discussed previously. This implies that a large number of trajectories has to be computed to simulate molecular beam experiments with random molecular orientation. TD-DFTB with its much lower numerical footprint allows to converge the relevant averages easily.

2 Time domain TD-DFTB and hole dynamics

Here we summarize the working equations of the real-time TD-DFTB method. Details on the derivation [16,17] and the general accuracy of the method [18–20] are available in the literature. We work in atomic units if not specified otherwise. The starting point of the method are the time-dependent Kohn–Sham equations

$$i\frac{\partial}{\partial t}|\psi_i(t)\rangle = \hat{H}|\psi_i(t)\rangle, \tag{1}$$

where the time-dependent Kohn–Sham states $|\psi_i(t)\rangle$ are expanded in a linear combination of atomic orbitals $|\phi_\mu\rangle$ centered on the atomic positions $\mathbf{R}_A$:

$$\psi_i(\mathbf{r},t) = \sum_\mu b_{\mu i}(t)\phi_\mu(\mathbf{r}-\mathbf{R}_A). \tag{2}$$

In this basis, the DFTB Hamiltonian is given by

$$H_{\mu\nu} = H^0_{\mu\nu} + \frac{1}{2}S_{\mu\nu}\sum_C(\gamma_{AC}+\gamma_{BC})\Delta q_C(t), \quad \mu\in A, \nu\in B. \tag{3}$$

DFTB is derived from an expansion of the DFT total energy around a given reference density ρ_0 (usually a sum of precomputed atomic densities) [16,21]. The zero-order term in this expansion gives rise to the term $\mathbf{H^0}$, while γ represents the electron-electron interaction in second order. $\mathbf{S}$ denotes the overlap matrix, while $q_A(t)$:

$$q_A(t) = \frac{1}{2}\sum_{i=1}^{N}\sum_{\mu\in A,\nu}\left(b^*_{\mu i}(t)b_{\nu i}(t)S_{\mu\nu} + b^*_{\nu i}(t)b_{\mu i}(t)S_{\nu\mu}\right), \tag{4}$$

are atomic Mulliken charges.

The term $\Delta q_A(t)$ in equation (2) is given by the difference of $q_A(t)$ and the number of valence electrons in the respective element. TD-DFTB incorporates the electron dynamics at the level of self-consistently updated charges instead of the full density as in conventional TD-DFT calculations. In this study we use the *mio-0-1* Slater-Koster set [21] that contains $\mathbf{H^0}$ and $\mathbf{S}$ evaluated for the PBE [22] exchange-correlation functional in tabulated form.

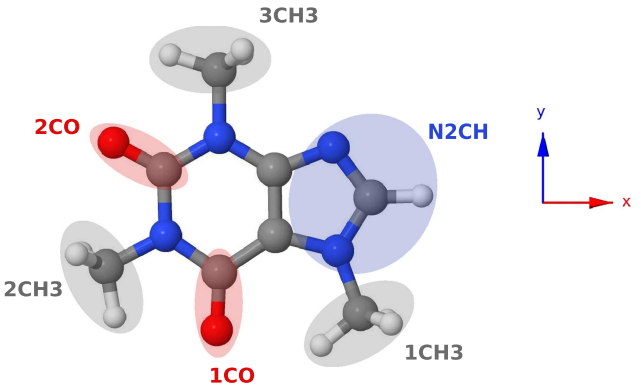

Fig. 1. DFTB lowest energy conformer of caffeine.

The target system for the numerical studies presented here is caffeine ($C_8N_4O_2H_{10}$) (Fig. 1), which features several functional groups that can possibly localize the hole density. Our choice is mainly motivated by the fact that pump-probe experiments for this system are currently carried out in our laboratory. Caffeine has several isomers that are characterized by rotations of the methyl groups and the various resulting H-bonding patterns with the carbonyl group oxygens. Ground state DFT simulations by Singh [23] indicate that the six lowest energy conformers are separated by only ≈ 6 kJ/mol and should therefore all be populated at room temperature. In the present study we focus on the lowest energy conformer at the DFTB level of theory depicted in Figure 1.

As a first application, we compute the hole dynamics in the *sudden ionization* limit [13], which is often employed in studies of charge migration [10,12,14]. To this end we first compute the electron density for the neutral N-electron system ($\rho_N(\mathbf{r})$) and remove one electron from a given molecular orbital (MO) in the corresponding Kohn–Sham determinant. This configuration is then taken as initial state for the propagation according to equation (1), which we perform using a norm-conserving Cayley algorithm with a time step of 2 au for a total of 80 fs. The time-dependent charge density is computed as $\rho_{N-1}(\mathbf{r},t) = \sum_i n_i|\psi_i(\mathbf{r},t)|^2$ with $\sum_i n_i = N-1$ and used to evaluate the hole density according to

$$\rho_{\text{hole}}(\mathbf{r},t) = \rho_N(\mathbf{r}) - \rho_{N-1}(\mathbf{r},t). \tag{5}$$

Figure 2 presents results for ionization out of selected MO. Shown is the hole charge on various functional groups that are defined in Figure 1. The hole charges are obtained from the density according to a Mulliken partitioning.

The first observation is that initially the hole is often localized on a specific functional group, which simply reflects the localization of the corresponding MO. This is followed by an ultrafast relaxation towards the rest of the molecule in less than 0.1 fs. This finding is in line with the

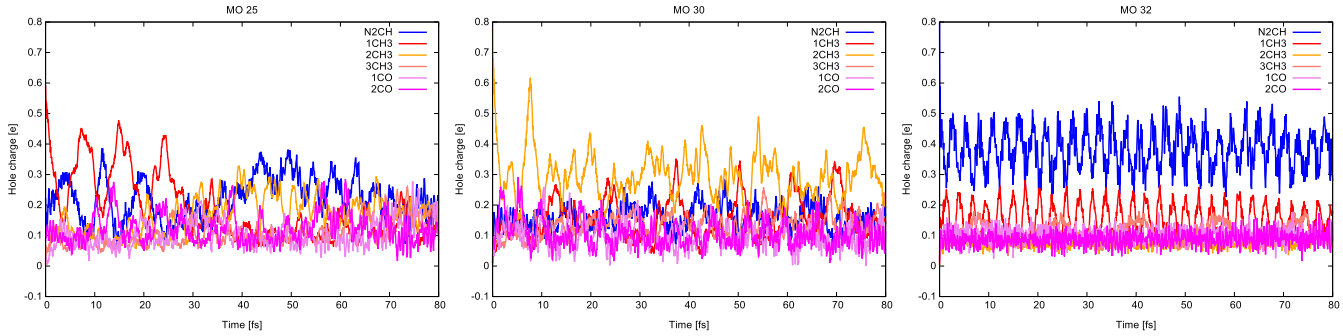

Fig. 2. Hole charges on various functional groups for sudden ionization out of MO n, for $n = 25$, 30 and 32. The index n labels valence orbitals with increasing orbital energy, the highest occupied molecular orbital (HOMO) having $n = 37$.

"universal time scale" for hole relaxation of 50 as, put forward by Breidbach and Cederbaum [24]. After the initial phase, the hole oscillates between different moieties of the molecule with different periods for the different ionized MO. As well known (see e.g. [10]), these dynamics originate from the fact that the initial state is not an eigenstate of the $N-1$ particle system and consequently characteristic quantum beats are observed. As seen in Figure 2, the hole dynamics for ionization out of different MO is completely different, both in terms of localization and temporal profile. It is therefore difficult to extract any further information without the precise knowledge of the ionizing laser pulse profile.

3 Complex absorbing potentials

In order to describe ionization in the present atomic orbital framework, we rely on the heuristic approach introduced by Klamroth and co-workers [25]. The basic idea is to add a purely imaginary potential $\Delta\hat{V}$ to the Hamiltonian:

$$\Delta\hat{V} = \frac{i}{2} \sum_{\{k:\,\epsilon_k>0\}} \Gamma_k |\bar{\psi}_k\rangle\langle\bar{\psi}_k|. \tag{6}$$

Here $|\bar{\psi}_k\rangle$ is an eigenstate of the Kohn–Sham Hamiltonian for the N-particle system with orbital energy ϵ_k and the sum runs over all unbound molecular orbitals with positive energy. The effect of this complex absorbing potential (CAP) is twofold. First, electrons excited to unbound orbitals will be drained from the system at a rate Γ_k. Second, the unbound levels are broadened and mimick in this way a continuum of states. As a result the ionization probability becomes a smooth function of the ionizing laser frequency. The rates Γ_k are further approximated as $\Gamma_k = \sqrt{\epsilon_k}/d$, where d is an empirical parameter. Since classically an electron in orbital k has a velocity $\sqrt{\epsilon_k}$, the parameter d can be interpreted as an escape length [25]. In the original article a value of $d = 1$ au was proposed. Using this choice, Sonk and Schlegel [26] found good agreement with experiment for the ratios of ionization rates of several polyenes. We therefore adhere to this value also in the present study.

While this approach offers the advantage of conceptual simplicity and ease of integration in every real-time electronic structure code that employs atomic orbitals, there are certainly also several disadvantages that should be mentioned. To start with, the unbound states are given as a linear combination of localized orbitals that do not resemble the plane wave characteristics of free, ionized electrons. Moreover, the ionization rates are obtained from a heuristic argument. Other choices for Γ_k are possible [27–30] and will lead to different ionization probabilities. Another drawback is based on the well known fact that Kohn–Sham orbital energies for conventional local/semilocal exchange-correlation functionals do not correspond to quasiparticle energies, i.e., the energies for electron removal or electron addition accounting for density relaxation. In fact, conventional functionals like the PBE used in this study exhibit a wrong asymptotic behaviour of the Kohn–Sham potential (see e.g. [31]). This leads to an underbinding of the outermost electrons and a strong violation of Koopmans' theorem. Specifically, the negative of the energy of the highest occupied MO underestimates the experimental ionization potential (IP) significantly. This is also the case for DFTB. We obtain $-\epsilon_{\mathrm{HOMO}} = 5.48\,\mathrm{eV}$, while the measured IP is 7.95 eV [32]. To circumvent this problem, we evaluate Γ_k by a rigid downwards shift of the DFTB orbital spectrum by this energy difference. As a result, MO 38 to MO 41 are unoccupied but bound in the ground state, while the remaining 25 orbitals represent the final states for ionization. Such a spectral shift is common practice in the DFT based computation of photoelectron spectra but serves only as ad-hoc solution for the underlying shortcomings of current functionals [33–35]. The recent development of range-separated functionals with proper asymptotic behaviour offers a better starting point [31,36–38]. While these functionals are now also available for the DFTB method [39–42], they are not yet incorporated in the present real-time TD-DFTB code.

In order to visualize the impact of the absorbing potential, we depict the absorption spectrum of Caffeine in Figure 3. The DFTB results have been obtained by applying a short δ-like field to the molecule and taking the Fourier transform of the induced dipole moment as discussed in references [17,43]. Results are shown with and without the CAP defined above. In the former case, we

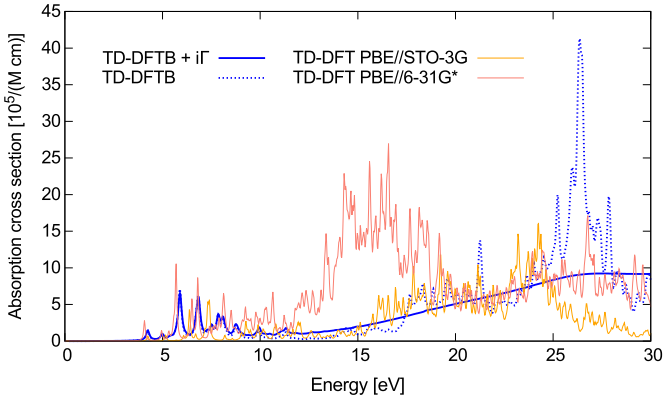

Fig. 3. Caffeine absorption cross section for TD-DFTB with and without CAP (termed iΓ) as well as TD-DFT first principles results (PBE) with different basis sets. The latter are Lorentzian broadened by 0.1 eV. The broadening in the TD-DFTB spectra arises from the finite simulation time and the complex absorbing potential.

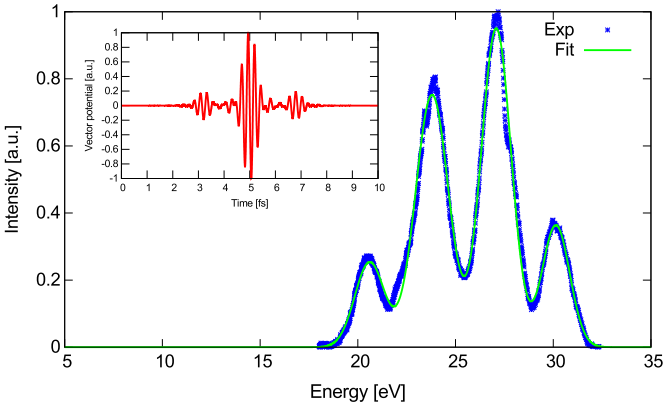

Fig. 4. Experimental pulse spectrum $I(\omega)$ and fit. The inset depicts the corresponding time dependent vector potential $A_0(t)$.

switch to a propagation algorithm (Euler) that is not explicitly norm conserving and reduce the time step to 0.1 au. For illustrative purposes we also show results for conventional TD-DFT calculations without CAP. These simulations were carried out with *NWCHEM* [44] (version 6.6) using the frequency domain Casida solver, the PBE functional and two different basis sets (STO-3G and 6-31G*).

The basic effect of the CAP is a strong broadening of the high energy part of the spectrum that washes out all fine details of the artificially discrete excited states. In the lower energy part (around 5 eV) several excitations are observed that are not affected by the CAP. These are due to transitions to bound virtual orbitals. For energies above the ionization potential, the broadening increases due to coupling with unbound orbitals and auto-ionizing resonances can be observed [27]. The agreement of TD-DFTB with the first-principles calculations with larger basis is quite reasonable in the low energy region. The large discrepancy between different levels of theory in the region 10–30 eV however highlights the known difficulties in obtaining continuum properties from localized atomic orbitals. While the application of a CAP does certainly not solve these convergence issues, it should strongly alleviate them.

4 Pulse profile and ionization probability

In order to incorporate the ionizing laser field into our simulations, we follow the work of Graf and Vogel [45], who gave an expression for the Hamiltonian in minimal coupling that is valid in the long wavelength limit:

$$H_{\mu\nu}[\mathbf{A}(t)] = \exp\left[i(\mathbf{R}_A - \mathbf{R}_B)\mathbf{A}(t)\right]H_{\mu\nu}; \quad \mu \in A, \nu \in B. \tag{7}$$

Even for the XUV pulses discussed here, the radiation wavelength is still much larger than the dimension of the molecule, such that this approximation is acceptable. Equation (7) relates the desired field dependent Hamiltonian to the already known matrix elements of the unperturbed one. We derive the actual vector potential from an experimental intensity spectrum $I(\omega)$. The latter has been obtained by a HHG setup to generate XUV pulses which has been described in detail elsewhere [46,47]. Figure 4 depicts the intensity of the pulse in the frequency domain. This spectrum is first fitted to a sum of four Gaussians centered at 20.5 eV, 24 eV, 27 eV and 30 eV, respectively. Fourier transformation and integration of the signal gives rise to the vector potential $A_0(t)$ in the inset. In the conversion we assumed that the pulse is band-width limited and consistent with a flat phase. The resulting field exhibits three short sub-pulses and a total duration of roughly 6 fs. We further scale $A_0(t)$ such that the peak intensity corresponds to 1.0×10^9 W/cm^2, the typical value found in the experiments. With these parameters, we solve the time-dependent Kohn–Sham equations and extract the ionization probabilities according to the prescription put forward by Ullrich [48] and later successfully used to quantify ionization yields in strong-field ionization of atoms [49].

During and after interaction with an ionizing laser pulse, the time-dependent many-body wave function Ψ_N for an N-particle system can generally be written in the following form:

$$\Psi_N(\mathbf{r}_1, \ldots, \mathbf{r}_N, t) = \sum_{k=0}^{N} \sum_j a_j^k(t) \bar{\Psi}_j^k(\mathbf{r}_1, \ldots, \mathbf{r}_N), \tag{8}$$

where $\bar{\Psi}_j^k$ denotes the jth eigenstate of the field-free many-body Hamiltonian with k electrons in the continuum and $N-k$ electrons attached to the molecule. The probabilities for finding the system in a charge state k are hence given by $P^k(t) = \sum_j |a_j^k(t)|^2$. Equation (8) can be turned into a practical scheme by further assuming that the many-body states $\bar{\Psi}_j^k$ can be reasonably approximated by Kohn–Sham determinants. This is clearly a significant drawback. For weak perturbations, however, $P^k(t)$ was

shown to be a functional of the total time-dependent density and is therefore exact in the framework of TD-DFT [48].

Furthermore, a criterion for the association of electrons to the continuum or to the molecule must be given. In reference [48] this problem was solved by defining an *analyzing box* $\mathcal{V}$ which encloses the molecule. The probability for an electron in the Kohn–Sham orbital $|\psi_i(t)\rangle$ to be bound is then simply given by

$$N_i(t) = \int_{\mathcal{V}} |\psi_i(\mathbf{r},t)|^2 \, d^3r, \tag{9}$$

and the probability for, .e.g., single ionization can be written in the following form:

$$P^1(t) = \sum_{i=1}^{N} N_1(t) \cdots \bar{N}_i(t) \cdots N_N(t), \tag{10}$$

with $\bar{N}_i = 1 - N_i$. This approach is well adapted to grid based TD-DFT implementations, where an *analyzing box* is easily realized. For our atomic orbital scheme there is no need to track the ejected electrons explicitly. We evaluate $N_i(t)$ instead by integration over all space. Under the influence of the laser pulse, the time-dependent Kohn–Sham states evolve into a coherent superposition of orbitals including the unbound ones. These are associated with the imaginary potential (Eq. (6)) which leads to a continuous loss of norm.

Figure 5 depicts results of simulations with the pulse form defined earlier for a polarization along the x-axis of the molecule. The ionization probability in the first 10 fs reflects directly the temporal profile of the pulse. After the pulse is over, P^1 remains constant and no further ionization takes place. For the parameters of the experimental setup, we are still in the linear regime as the results for doubled intensity show. This can also be quantified by evaluating $P^n(t)$ for $n > 2$, which does not exceed 10^{-9}. Coming back to the absorption cross sections in Figure 3, it seems likely that DFTB overestimates the ionization yield. In fact, the pulse is localized around 25 eV in frequency space, a region where DFTB shows a much larger cross section than the first-principles calculations with reasonably sized basis.

5 Laser induced hole dynamics

Next, we attempt to evaluate the electron density of the cation from the time-dependent Kohn–Sham state. The approach presented here is very similar to the work of Lara-Astiaso et al. [15], who use time-dependent perturbation theory together with multicenter B-spline basis functions to model the continuum. Apart from this different treatment of the continuum states, we obtain the time-dependent Kohn–Sham states from numerical real-time propagation which is in principle also valid in the high intensity limit.

First, we construct a density matrix for the $(N-1)$ particle system by tracing over the unbound single-particle

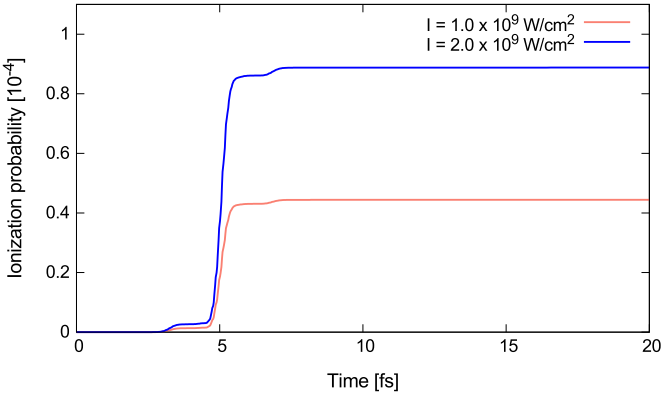

Fig. 5. Probability of single ionization $P^1(t)$ for light polarization along the x-axis and different intensities. For $I = 1.0 \times 10^9$ W/cm^2 approximately 4.5×10^{-5} electrons leave the system.

Kohn–Sham states:

$$\hat{\Gamma}_{N-1}(t) = \frac{1}{F} \sum_{\{k:\,\epsilon_k>0\}} \langle\bar{\psi}_k|\Psi_N(t)\rangle\langle\Psi_N(t)|\bar{\psi}_k\rangle, \tag{11}$$

where the normalizing factor F ensures that the density integrates to the correct number of particles. Assuming further that the time-dependent many-body state $|\Psi_N(t)\rangle$ can be approximated by the Kohn–Sham determinant $|\psi_1(t),\ldots,\psi_N(t)\rangle$, one arrives at the following expression for the cationic electron density ρ_{N-1}:

$$\rho_{N-1}(\mathbf{r},t) = \frac{1}{F}\left\{\sum_{i=1}^{N} D_{ii} \sum_{\substack{j=1\\ j\neq i}}^{N} |\psi_j(\mathbf{r},t)|^2 + \sum_{i=1}^{N}\sum_{j=1}^{N} D_{ij}\psi_i^*(\mathbf{r},t)\psi_j(\mathbf{r},t)\right\}, \tag{12}$$

with $F = N\,\mathrm{tr}(\mathbf{D})/(N-1)$. The matrix $\mathbf{D}$ is defined by the expansion of the time-dependent Kohn–Sham states into the set of ground state Kohn–Sham states:

$$|\psi_i(t)\rangle = \sum_{k=1}^{N} d_{ik}(t)|\bar{\psi}_k\rangle \tag{13}$$

$$D_{ij} = \sum_{\{k:\,\epsilon_k>0\}} d_{ik}^*(t) d_{jk}(t). \tag{14}$$

Equation (12) can be used to evaluate the hole density as done previously (Eq. (5)), but this time the ionizing pulse profile is fully taken into account.

One consequence of this explicit inclusion is a strong dependency of the observed hole dynamics on the light polarization. In fact, a certain molecular orbital i contributes strongly to the hole density if the transition amplitude d_{ik} to a continuum state is sizable. This in return is based on the dipole matrix elements between

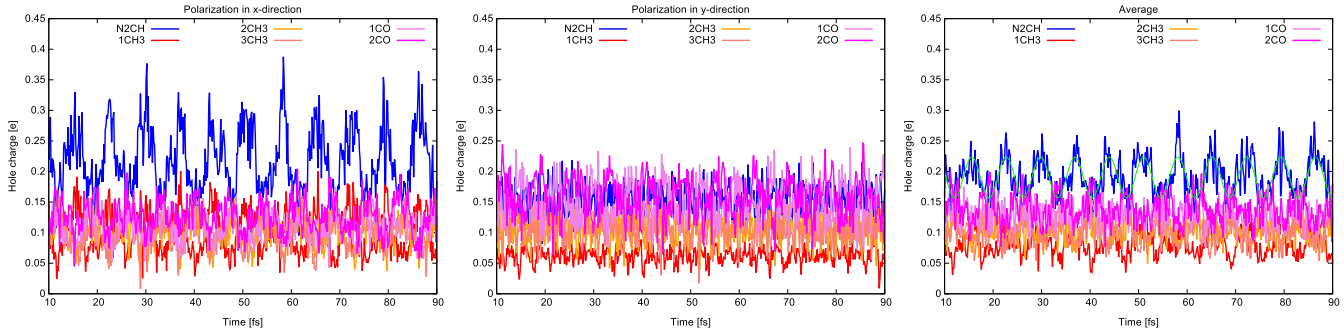

Fig. 6. Hole charges on various functional groups after ionization with a 10 fs laser pulse with intensity $I = 1.0 \times 10^9$ W/cm^2. The left plot show the results for laser polarization in the x-direction, the middle plot the same for polarization in the y-direction, while the right plot show the orientational average over 180 trajectories. The green line serves as guide to the eye for the partial hole charge on the N2CH group.

these states and hence very dependent on the orientation of the molecule with respect to the polarization of the laser. Given that Caffeine is randomly oriented in the molecular beam, we therefore have to average the hole density over the possible realizations of the polarization.[1] Figure 6 shows an average over 180 trajectories with varying polarization in the molecular xy-plane for a fixed intensity of $I = 1.0 \times 10^9$ W/cm^2. We do not consider excitation in z-direction since it does not lead to appreciable ionization. As can be seen, the resulting charge dynamics do not resemble the results for sudden ionization out of an individual molecular orbital. Instead, the hole dynamics is given by a complex superposition of these traces governed by the shape and temporal profile of the laser pulse. Interestingly, one still observes oscillatory features even after averaging. The charge on the N2CH group migrates mostly to the 2CO group on a time scale of roughly 7 fs. We note that the hole dynamics remains virtually unchanged when we double the pulse intensity. This indicates that the projection on the $N-1$ particle state in equation (11) provides internally consistent results.

6 Conclusions

Several aspects of the methodology presented here are clearly outside the typical *comfort zone* of TDDFT calculations. This includes the treatment of the continuum by localized orbitals plus a heuristically motivated CAP as well as the indentification of many-body wave functions with simple Kohn–Sham determinants in various places. While the error brought upon by these approximations is difficult to assess, the main findings of this work are intuitive and expected to be general. The physical picture of a sudden removal which is often employed to motivate ionization out of a single MO is questionable in the context of present attosecond pump-probe setups. In fact, the observed charge dynamics depends on the specific time profile of the ionizing laser pulse and resembles none of the individual MO hole densities. It is better described as correlated electron dynamics due to a coherent superposition of ionic states. Due to this field dependence, charge migration also depends on the molecular orientation and comparison to experimental observables requires proper orientational sampling. For caffeine, we found that characteristic charge oscillations survive this process and might be detectable. A natural question then arises whether nuclear motion might spoil the remaining signature of charge migration. Several groups already worked on this topic [15,51,52], although not including the mentioned dependence on pulse profile and molecular orientation. The present TD-DFTB based method lends naturally to an Ehrenfest approach for electron-ion dynamics [16]. Here it would be necessary to evaluate the forces stemming from the projected $N-1$ particle density instead of the N-particle density which stays always close to the ground state for weak field ionization. Work in this direction is currently in progress.

T.N. would like to thank the *Laboratoire d'Excellence iMUST* and the fund *BQR Accueil EC 2016* for financial support. K. Y. is grateful for the financial supports from Building of Consortia for the Development of Human Resources in Science and Technology by the Ministry of Education, Culture, Sports, Science and Technology (MEXT).

Author contribution statement

T. Niehaus, K. Yamazaki and F. Lepine designed the research project together. T. Niehaus carried out the calculations with the help of M. Meziane. F. Lepine and A. Marciniak provided the experimental data. All authors contributed to data interpretation and discussion of the results, while T. Niehaus finally wrote the manuscript. All the authors have read and approved the final version of the article.

References

1. E. Runge, E.K.U. Gross, Phys. Rev. Lett. **52**, 997 (1984)
2. S. Meng, J. Ren, E. Kaxiras, Nano Lett. **8**, 3266 (2008)

[1] See [50] for a recent experiment in which the molecular orientation could be controlled.

3. T. Otobe, M. Yamagiwa, J.I. Iwata, K. Yabana, T. Nakatsukasa, G.F. Bertsch, Phys. Rev. B **77**, 165104 (2008)
4. A.H. Zewail, Angew. Chem. Int. Ed. **39**, 2586 (2000)
5. R. Weinkauf, P. Schanen, D. Yang, S. Soukara, E. Schlag, J. Phys. Chem. **99**, 11255 (1995)
6. L. Lehr, T. Horneff, R. Weinkauf, E. Schlag, J. Phys. Chem. A **109**, 8074 (2005)
7. L. Belshaw, F. Calegari, M.J. Duffy, A. Trabattoni, L. Poletto, M. Nisoli, J.B. Greenwood, J. Phys. Chem. Lett. **3**, 3751 (2012)
8. F. Lépine, G. Sansone, M.J. Vrakking, Chem. Phys. Lett. **578**, 1 (2013)
9. F. Calegari et al., Science **346**, 336 (2014)
10. L.S. Cederbaum, J. Zobeley, Chem. Phys. Lett. **307**, 205 (1999)
11. J. Breidbach, L. Cederbaum, J. Chem. Phys. **118**, 3983 (2003)
12. A.I. Kuleff, L.S. Cederbaum, J. Phys. B: At. Mol. Opt. Phys. **47**, 124002 (2014)
13. H.W. Meldner, J.D. Perez, Phys. Rev. A **4**, 1388 (1971)
14. F. Remacle, R. Levine, Proc. Natl. Acad. Sci. **103**, 6793 (2006)
15. M. Lara-Astiaso, D. Ayuso, I. Tavernelli, P. Decleva, A. Palacios, F. Martin, Faraday Discuss. **194**, 41 (2016)
16. T.A. Niehaus, D. Heringer, B. Torralva, T. Frauenheim, Eur. Phys. J. D **35**, 467 (2005)
17. T.A. Niehaus, J. Mol. Struct.: THEOCHEM **914**, 38 (2009)
18. T.A. Niehaus, S. Suhai, F. Della Sala, P. Lugli, M. Elstner, G. Seifert, T. Frauenheim, Phys. Rev. B **63**, 085108 (2001)
19. F. Trani, G. Scalmani, G. Zheng, I. Carnimeo, M. Frisch, V. Barone, J. Chem. Theory Comput. **7**, 3304 (2011)
20. A. Dominguez, B. Aradi, T. Frauenheim, V. Lutsker, T.A. Niehaus, J. Chem. Theory Comput. **9**, 4901 (2013)
21. M. Elstner, D. Porezag, G. Jungnickel, J. Elsner, M. Haugk, T. Frauenheim, S. Suhai, G. Seifert, Phys. Rev. B **58**, 7260 (1998)
22. J. Perdew, K. Burke, M. Ernzerhof, Phys. Rev. Lett. **77**, 3865 (1996)
23. V.B. Singh, RSC Adv. **4**, 58116 (2014)
24. J. Breidbach, L. Cederbaum, Phys. Rev. Lett. **94**, 033901 (2005)
25. S. Klinkusch, P. Saalfrank, T. Klamroth, J. Chem. Phys. **131**, 114304 (2009)
26. J.A. Sonk, H.B. Schlegel, J. Phys. Chem. A **116**, 7161 (2012)
27. K. Lopata, N. Govind, J. Chem. Theory Comput. **9**, 4939 (2013)
28. P. Krause, J.A. Sonk, H.B. Schlegel, J. Chem. Phys. **140**, 174113 (2014)
29. T. Sommerfeld, M. Ehara, J. Chem. Theory Comput. **11**, 4627 (2015)
30. J.J. Goings, P.J. Lestrange, X. Li, Wiley Interdiscip. Rev. Comput. Mol. Sci. **8**, e1341 (2018)
31. R. Baer, E. Livshits, U. Salzner, Annu. Rev. Phys. Chem. **61**, 85 (2010)
32. D. Dougherty, E. Younathan, R. Voll, S. Abdulnur, S. McGlynn, J. Electron Spectrosc. Relat. Phenom. **13**, 379 (1978)
33. M. Moseler, B. Huber, H. Häkkinen, U. Landman, G. Wrigge, M.A. Hoffmann, B.v. Issendorff, Phys. Rev. B **68**, 165413 (2003)
34. L. Kronik, R. Fromherz, E. Ko, G. Ganteför, J.R. Chelikowsky, Nat. Mater. **1**, 49 (2002)
35. T. Körzdörfer, S. Kümmel, Phys. Rev. B **82**, 155206 (2010)
36. T. Leininger, H. Stoll, H.J. Werner, A. Savin, Chem. Phys. Lett. **275**, 151 (1997)
37. S. Refaely-Abramson, S. Sharifzadeh, N. Govind, J. Autschbach, J.B. Neaton, R. Baer, L. Kronik, Phys. Rev. Lett. **109**, 226405 (2012)
38. L. Kronik, S. Kümmel, in *First principles approaches to spectroscopic properties of complex materials*, Topics of Current Chemistry, edited by C. di Valentin, S. Botti, M. Coccoccioni (Springer, Berlin, 2014), Vol. 347 pp. 137–192
39. T. Niehaus, F. Della Sala, Physica Status Solidi (b) **249**, 237 (2012)
40. V. Lutsker, B. Aradi, T.A. Niehaus, J. Chem. Phys. **143**, 184107 (2015)
41. A. Humeniuk, R. Mitrić, J. Chem. Phys. **143**, 134120 (2015)
42. J.J. Kranz, M. Elstner, B. Aradi, T. Frauenheim, V. Lutsker, A.D. Garcia, T.A. Niehaus, J. Chem. Theory Comput. **13**, 1737 (2017)
43. K. Yabana, G. Bertsch, Phys. Rev. B **54**, 4484 (1996)
44. M. Valiev, E.J. Bylaska, N. Govind, K. Kowalski, T.P. Straatsma, H.J. Van Dam, D. Wang, J. Nieplocha, E. Apra, T.L. Windus, W.A. de Jong, Comput. Phys. Commun. **181**, 1477 (2010)
45. M. Graf, P. Vogl, Phys. Rev. B **51**, 4940 (1995)
46. A. Marciniak, V. Despré, T. Barillot, A. Rouzée, M. Galbraith, J. Klei, C.H. Yang, C. Smeenk, V. Loriot, S.N. Reddy, A. Tielens, S. Mahapatra, A. Kuleff, M. Vrakking, F. Lépine, Nat. Commun. **6**, 7909 (2015)
47. A. Marciniak, Dynamique électronique femtoseconde et sub-femtoseconde d'édifices moléculaires complexes superexcités, Ph.D. thesis, Université de Lyon, 2016
48. C. Ullrich, J. Mol. Struct. THEOCHEM **501**, 315 (2000)
49. A. Crawford-Uranga et al., Phys. Rev. A **90**, 033412 (2014)
50. P.M. Kraus, B. Mignolet, D. Baykusheva, A. Rupenyan, L. Horný, E.F. Penka, G. Grassi, O.I. Tolstikhin, J. Schneider, F. Jensen, L.B. Madsen, A.D. Bandrauk, F. Remacle, H.J. Wörner, Science **350**, 790 (2015)
51. M. Vacher, D. Mendive-Tapia, M.J. Bearpark, M.A. Robb, J. Chem. Phys. **142**, 094105 (2015)
52. A.J. Jenkins, M. Vacher, R.M. Twidale, M.J. Bearpark, M.A. Robb, J. Chem. Phys. **145**, 164103 (2016)